Carbon xxx (2018) xxx-xxx

Contents lists available at ScienceDirect

Carbon

journal homepage: www.elsevier.com

Additive-free electrode fabrication with reduced graphene oxide using supersonic kinetic spray for flexible lithium-ion batteries

Seong Dae Kim[a], Jong-Gun Lee[b, 1], Tae-Gun Kim[b], Kuldeep Rana[c], Jong Yeob Jeong[d], Jong Hyeok Park[d], Sam S. Yoon[b], Jong-Hyun Ahn[a, *]

[a] School of Electrical and Electronic Engineering, Yonsei University, 50 Yonsei-ro, Seoul, 03722, Republic of Korea
[b] School of Mechanical Engineering, Korea University, 145 Anam-ro, Seoul, 02841, Republic of Korea
[c] Electrical Appliances Technology Division, Central Power Research Institute, Prof, Sir CV Raman Road, Bangalore, Karnataka, 560080, India
[d] Department of Chemical and Biomolecular Engineering, Yonsei University, 50 Yonsei-ro, Seoul, 03722, Republic of Korea

ARTICLE INFO

Article history:
Received 13 March 2018
Received in revised form 14 May 2018
Accepted 15 June 2018
Available online xxx

Keywords:
Lithium ion batteries
Reduced graphene oxide
Adhesion energy
Flexible energy storages
Flexible electronics

ABSTRACT

Thin, lightweight, and flexible lithium-ion batteries (LIBs) are emerging as a promising power source for high-performance flexible electronics. However, their technological drawbacks have hindered the development of fully flexible electronics because of a lack of reliable electrode materials that combine superior electrochemical properties with mechanical flexibility. As a solution to this problem, we herein demonstrate an additive-free electrode fabrication process, where reduced graphene oxide (rGO) is coated onto a current collector using a supersonic kinetic spray technique (spray-rGO). The spray-rGO demonstrates outstanding mechanical and electrochemical properties compared to those of rGO electrodes fabricated using the conventional process. Moreover, despite being fabricated without any binders, spray-rGO exhibits high adhesion energy, which enables the fabrication of highly flexible electrodes with no structural deterioration or capacity degradation. This approach to fabricate additive-free flexible electrodes, which results in electrodes that satisfy other important criteria such as high rate capability, long-term cyclability, and facile and fast fabrication, is a prospective method for developing high-performance flexible LIBs.

1. Introduction

Flexible, stretchable, and wearable electronic devices are being actively investigated as emergent and promising next-generation technologies [1–6]. However, several issues facing the development of flexible energy storage devices for powering electronics in a flex/bent state are yet to be overcome [7,8]. Flexible energy storage devices must demonstrate essential electrochemical and mechanical characteristics such as high capacity, high rate capability, long cycle life, low cost, and high flexibility.

Currently, lithium-ion batteries (LIBs) dominate the market because of their properties such as high rate capability, high energy density, and long cycle life [9,10]. The fabrication processes of LIB electrodes involve coating slurry onto a metal current collector, where the slurry comprises a mixture of an active material, a conductive agent, and a binder. However, the application of such devices as flexible batteries in flexible electronic devices has been limited because of unreliable or improper electrode materials and fabrication processes. Various issues with conventional LIB electrodes need to be resolved for them to be used in flexible batteries. The first problem is weak adhesion at the interface between the electrode materials and the current collector because of the point contact formed by only binder particles [11,12]. Electrodes with weak adhesion can develop cracks and delamination at the interface because of deformation in the bent/flex state and volumetric expansion during repeated charge and discharge, resulting in capacity loss and performance deterioration. Among the other constraints, the additives, which are approximately 5%–10% of the total weight of the electrodes, are not electrochemically active, and thus, do not store Li^+ ions, thereby reducing the overall gravimetric capacity. Furthermore, additives can result in degradation of electrochemical performance. The irreversible capacity increases with increasing additive content in the electrode materials [13,14]. Such issues with additives have been a main constraint in developing fully flexible LIBs. Therefore, a novel process that ensures high adhesion energy and compensates for the capacity loss due to additives would enable the fabrication of flexible electrodes for flexible LIBs.

In this regard, several approaches for solving the aforementioned issues related to additives and adhesion-energy problems for flexible LIBs have been reported. In some approaches, the surface of a current collector was roughened by a surface treatment such as a porous Cu foil or nanostructure growth over the surface to increase the adhesion energy at the interface [15–18]. Other approaches include use of nonmetallic current collectors with higher adhesion energy, such as graphite sheets, carbon fibers, or carbon paper [19–27]. Even though these approaches improves the adhesion energy at the interface, the

* Corresponding author.
Email address: ahnj@yonsei.ac.kr (J-H Ahn)
[1] Current address: NanoEngineering Group, Faculty of Mechanical Engineering, Technion-Israel Institute of Technology, Haifa, 32000.

https://doi.org/10.1016/j.carbon.2018.06.040
0008-6223/

fundamental problems of detachment and additive content have not been resolved. On the other hand, additive-free electrode fabrication such as vacuum filtration, chemical vapor deposition (CVD), and hydrothermal synthesis methods have been investigated [28–33]. However, these approaches have complicated processing steps and do not result in electrodes that simultaneously satisfy all necessary characteristics for use in flexible LIBs (e.g., high rate capability, long lifetime, and mechanical flexibility). Hence, a facile electrode fabrication process that yields electrodes that fulfil all requirements for flexible LIBs is urgently needed.

Herein, we describe a novel method for the fabrication of an additive-free reduced graphene oxide (rGO) electrode using the supersonic kinetic spray technique (spray-rGO) [34] and successfully demonstrate its incorporation into a flexible LIB. Because the supersonic kinetic spray imparts high energy to the particles, the coated rGO film enables direct coating and exhibits a self-healing effect. However, the most widely used anode material, graphite, is not suitable for use in the spray process because its large particles size results in a poor coating efficiency. By contrast, rGO particles, which are produced through a chemical exfoliation process from graphite, are much smaller than graphite particles, making them suitable for use in the supersonic kinetic spray process. Moreover, rGO possesses various outstanding properties, including excellent conductivity, large surface area, and high lithium-ion diffusivity ($\sim 10^{-7}$ to $10^{-6}\,cm^2\,s^{-1}$), indicating suitable characteristics for use in high-power LIBs [35]. Therefore, using supersonic kinetic and rGO particles, we have fabricated an additive-free rGO electrode. Among the various improved properties of the spray-rGO electrode, it exhibits better adhesion energy than an rGO electrode fabricated by the conventional slurry method (slurry-rGO) because of the large contact area at the interface between the electrode and the current collector; thus, its properties render it suitable for use in flexible LIBs. Moreover, the spray-rGO electrode shows better electrochemical performance, including better rate capability and long-term cyclability than slurry-rGO. The mechanical flexibility of spray-rGO is successfully demonstrated via improved adhesion energy in flexible LIBs when the batteries are bent and twisted severely. Because this proposed method increases the adhesion energy without using any binders, this novel electrode fabrication process will facilitate the future development of flexible LIBs with broad potential application.

2. Experimental section

2.1. Fabrication of spray-rGO and slurry-rGO

The precursor suspension for the spray-rGO coating process was prepared by mixing 0.8 g of rGO (product name: N002-PDR; size < 10 μm; Angstrom Company) in a 40 mL solution of isopropyl alcohol (Samjeon Chem.) and dimethylformamide (Sigma-Aldrich) (3:1 ratio in v/v). The dispersive solution was sonicated for 2 h to form a uniform rGO suspension. After confirming by visual inspection that the rGO suspension was free of precipitates, we fabricated the rGO electrode (without using a binder) on the Cu current collector by injecting the solution using a supersonic kinetic spray [34]. The detailed parameters used for the spray-coating process were as follows: pressure of 4 bar, nozzle temperature of 300 °C, flow rate of $3.0\,mL\,min^{-1}$ using a 50 mL syringe, and 10 sweeps per syringe to produce a thick and uniform coating for use as an LIB electrode. The thickness of the coating after the spraying process was approximately 15 μm. This coated electrode was directly used as an anode for LIBs in coin cells and in flexible LIBs without any additional treatment such as a cleaning, aging, or thermal treatment.

The slurry-rGO was prepared by mixing of rGO with the carbon black super-P (Timcal Ltd.,) as a conducting agent, and poly(vinylidone difluoride) (PVDF) in N-methyl-2-pyrrolidone (NMP) solvent with the weight ratio of 90:7:3. The mixing of the materials was carried out for almost 1 h in order to form uniform distribution of active materials with additives. The mixed slurry was then coated on the Cu current collector uniformly. After coating, the slurry-rGO on Cu-current collector was dried at 80 °C in a vacuum oven for more than 12 h to evaporate solvent.

The loaded mass for both slurry-rGO and spray-rGO was about $100\,g/m^2$; however, the exact loaded mass of rGO materials in slurry-rGO was 90% of total slurry weight (i.e. $90\,g/m^2$) and the other portion (~10%) was additives. Due to additive-free fabrication process, the gravimetric capacity of spray-rGO shows about 10% more than that of slurry-rGO.

2.2. Adhesion energy measurements

A force station (Physionics Co., Ltd.)-based adhesion test system was used to measure and compare the adhesion energy of spray-rGO and slurry-rGO on Cu current collectors. The structural configuration for adhesion measurements was as follows: From bottom to top, the lower part for sustaining the electrode on the stage consisted of stage/double-sided tape/supporting and handling glass substrate/double-sided tape/target electrode of spray-rGO or slurry-rGO on a Cu current collector. The upper part for measuring adhesion energy consisted of double-sided tape/supporting and handling glass substrate/double-sided tape/driving unit of the force station. The area of the upper double-sided tape, which directly contacted the electrode surface, was limited to 1 cm × 1 cm to ensure that each electrode had the same exposed area. The measurement sequence involved two steps of pressing and pulling. Initially, after a force of 20 N was applied to make fine contact between the upper tape and the electrode surface, various parameters such as displacement, force, and time were simultaneously measured by the force station as the pulling force was increased.

2.3. Material characterization

Raman spectroscopy (Horiba, Lab Ram ARAMIS) was used to characterize the self-healing effect of the supersonic kinetic spray on spray-rGO. Field-emission scanning electron microscopy (JEOL, JSM-7001F) was used to observe the morphology of the surface and the thickness of spray-rGO. For the cross-section observations, the edges were cleanly cut using a cross-section polisher (CP, JEOL, IB-19510CP). Electrochemical measurements such as cyclic voltammogram, charge/discharge profiles, cycle performance, rate capability, and electrochemical impedance spectroscopy (EIS) were carried out with assembled coin cells. The coin cells were assembled inside an Ar-filled glove box in which the O_2 and moisture concentrations were both less than 5 ppm. The spray-rGO/slurry-rGO and Li metal served as the working electrode and the counter/reference electrode, respectively. A polyethylene (PE) film was used as a separator to prevent an electrical short between the two electrodes. The electrolyte, which served as a carrier for Li^+ ions between the two electrodes, consisted of 1 M $LiPF_6$ solution in a 1:1 (v/v) mixture of ethylene carbonate and dimethyl carbonate. Electrochemical measurements such as cyclic voltammogram for evaluating half cells and flexible LIBs were carried out using a battery cycler (Won-A Tech, WBCS 3000) with cut-off voltages of 0–2.7 V and 0–2.5 V [36]. EIS was conducted using a potentiostat (Won-A Tech, Zive-sp1) in the frequency range of $\sim 10^{-3}$ to 10^6 Hz [28].

2.4. Flexible LIBs assembly

Flexible lithium ion battery was fabricated by using PDMS substrate in the configuration of PDMS/spray-rGO anode/separator/LCO cathode/PDMS, which structure can be bent and twisted. The cathode and anode were separated by a polypropylene film in order to avoid short circuit, which is conducting for the lithium ions but insulator for electrons. After assembling the flexible battery, the electrolyte was injected using the syringe. Finally, the flexible battery was sealed by using PDMS, the whole processes of assembling of flexible battery were carried out in Ar-filled glove box. The method of fabricating flexible LIB using slurry-rGO was the same as that of flexible LIB using spray-rGO.

3. Results and discussion

The overall process of the supersonic kinetic spray coating used to fabricate additive-free electrodes is shown in Fig. 1a. First, the rGO suspension was prepared in a 50-mL syringe and injected as a source material for a spray-rGO electrode at a precise injection rate using a syringe pump. A high-pressure air stream was spewed through the supersonic nozzle and injected rGO particles toward the current collector. The flow of high-pressure air increased the kinetic energy of the rGO particles and aided in evaporation of the solvent used for the suspension [34]. The thickness of spray-rGO can be controlled by changing the concentration of the rGO suspension and by repeating the coating cycles. The density and coating efficiency depend on the injection rate of the suspension velocity of the air stream, the temperature of the supersonic nozzle, and the distance between the nozzle and the target substrate [34].

Through a series of mixing and spraying processes, an additive-free spray-rGO electrode was successfully produced under high kinetic energy. The processes involved two steps: dispersive solution mixing and supersonic spray-coating. As shown in the inset of Fig. 1a, the Cu current collector was uniformly coated with sprayed rGO particles. The cross-sectional SEM images in Fig. S1 confirm that the spray-rGO electrode had microscale thickness similar to that of the slurry-rGO electrode. The thickness of the spray-rGO electrode could be controlled as required for high-power or high-energy-density LIB applications.

Previously, a supersonic spray method for film formation was demonstrated to result in rGO with a self-healing effect [34]. In the present study, we used Raman spectroscopy, which is a nondestruc-

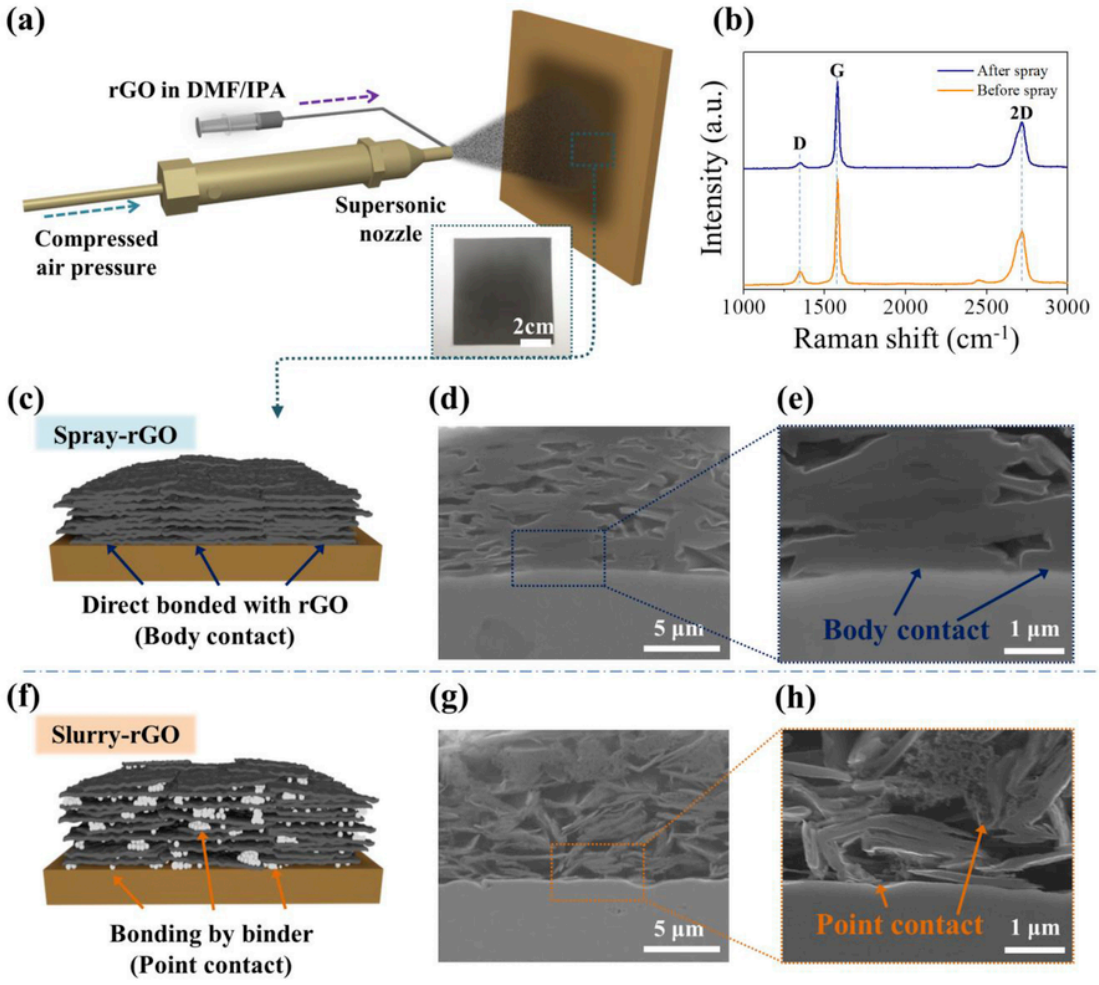

Fig. 1. (a) Overall schematic of additive-free coating of an rGO electrode using supersonic kinetic spraying. The inset shows an optical image of spray-rGO. (b) Raman spectra of spray-rGO and slurry-rGO in the frequency range of 1000–3000 cm^{-1}. (c) Schematic structure of spray-rGO. (d–e) Cross-sectional SEM images of spray-rGO with different magnifications. (f) Schematic structure of slurry-rGO. (g–h) Cross-sectional SEM images of slurry-rGO with different magnifications. (A colour version of this figure can be viewed online.)

tive method, to determine whether the self-healing effect persists for a microscale stacked rGO film on a Cu current collector. Fig. 1b shows the Raman spectra of rGO before and after coating by the spray method. The Raman spectra consist of D peaks (~1350 cm^{-1}), G peaks (~1580 cm^{-1}), and 2D peaks (~2700 cm^{-1}), which are typical peaks of graphitic material such as graphite, graphene and rGO [37]. The presence of the characteristic peaks of carbon materials in the Raman spectra confirms the self-healing effect in spray-rGO [34]. The position of the G peak, which is associated with the double-degenerate E_{2g} mode, slightly shifted from 1580 cm^{-1}–1578 cm^{-1} after the spray process. The 2D peak, which appears because of the second-order zone boundary phonons, shifted from 2718 cm^{-1}–2716 cm^{-1}.[33] That is, because of the high-energy impact of the supersonic kinetic spray process, the rGO particles were subjected to in-plane stretching forces, resulting in a self-healing effect upon the change from Stone–Wales defects [5-7-7-5 ring structure] and C2 vacancies [5-8-5 ring structure] to an ideal hexagonal structure [34,39]. In addition, the intensity ratio between the D and G peaks (I_D/I_G), which is a criterion for evaluating the defect level, was 0.166 for the pristine rGO particles and decreased to 0.112 after the spraying process. When carbon-based materials are used as an anode material in LIBs, retained defects such as impurities or vacancies can increase in the initial specific capacity; however, an increased defect level in rGO can hinder battery performance with respect to, for example, reversible capacity, long-term cyclability, and stability, which are essential properties for flexible LIBs [40,41]. That is, a lower I_D/I_G in the Raman spectra of spray-rGO indicates that it contains fewer defects than pristine rGO particles, which can result in improved essential properties of flexible LIBs. Thus, the Raman spectra confirmed the integrity of deposited rGO particles coated with high velocity and indicated that this approach is applicable to the coating of various films onto current collectors.

An important aspect of using the supersonic kinetic spray method for electrode fabrication is the ability to fabricate an rGO electrode without binders, which function only as construction agents. In the spraying process, direct deposition of the rGO layer onto the current collector could enable the fabrication of binder-free electrodes. We investigated the structural differences between spray-rGO and slurry-rGO using SEM; the resulting images are shown in Fig. 1c–h. Fig. 1c shows that the spray-rGO electrode formed without a binder on the current collector exhibits direct contact and has a large contact area at the interface. For a more detailed observation and direct evidence, we collected cross-sectional SEM images of spray-rGO; one such image is shown in Fig. 1d. The rGO particles were well stacked in the absence of an adhesive agent and exhibited large and direct contact with the current collector. The SEM image in Fig. 1e is a high-magnification image that clearly shows the interface between the rGO electrode and the current collector and confirms plane contact at the interface. A schematic of the slurry-rGO structure prepared by the conventional slurry-based process is shown in Fig. 1f. In this case, only binder particles held the rGO particles and formed an adhesive surface at the interface. Moreover, as shown in Fig. 1g–h, slurry-rGO was bonded by binder particles via point contact, whereas the large regions without binder were not closely packed, resulting in poor connectivity between the electrode and current collector.

The adhesion energy at the interface is an important factor for the application of an electrode in flexible LIBs [12]. If the adhesion energy is insufficient, delamination and chipping-off in flex states can occur at the interface between the electrode and current collector. The abnormal performance of nonflexible electrodes in flexible energy storage devices results in performance degradation because of the reduced contact area and a loss of active material. To confirm the adhesion energy of the binder-free spray-rGO and slurry-rGO on Cu current collectors, we directly measured the adhesion energy using a force station to apply pulling/pressing force while measuring the displacement, time, and force simultaneously. Fig. 2a shows a schematic of the force-station adhesion measurement system for the rGO electrodes. The configuration of the lower part, from bottom to top, was moving stage/glass substrate/current collector/rGO electrode. For the upper part, an auxiliary glass substrate was attached to the upper force-station driving part and an adhesive layer was formed with an adhesive tape on the lower surface of the glass to make adhesive contact with the rGO electrode. The adhesion energies of spray-rGO and slurry-rGO were measured using a constant area of 1 cm × 1 cm formed with the adhesive layer at the upper part of the electrodes.

Figure S2 explains the process sequence of adhesion energy measurements in terms of time vs. pressing/pulling force. At the early stage of measurement, a pressing force of ~20 N was applied to form a conformal contact between the upper adhesive layer and the electrode surface with uneven roughness. The pulling force was then applied, and the adhesion force, displacement, and time were simultaneously measured (Fig. 2b). We observed that the pulling force applied to the electrode increased with displacement and that the adhesion energy prevented separation until detachment occurred. That is, the measured force value indicated that the adhesion energy had a limitation force that can be sustained at the point where detachment occurs. Upon completion of the process, the adhesion energy values for spray-rGO and slurry rGO were determined to be approximately 210 and 106 kPa, respectively. Thus, spray-rGO resulted in a two-fold increase in adhesion energy compared to slurry-rGO because of its larger contact area, as confirmed in the cross-sectional SEM images. Fig. 2c and d shows schematics of the difference between adhesion energy measurements of spray-rGO and slurry-rGO and photographs of the electrodes and double-sided tape located in the upper part. In this regard, the extent of electrode delamination differed. In the case of spray-rGO, only the upper part of the electrode was peeled-off because the adhesion energy between the rGO electrode and current collector was likely higher than the cohesion energy within the rGO electrode. By contrast, in the case of slurry-rGO, more rGO electrode was delaminated, possibly because of the rGO particles' lower adhesive energy and the smaller contact area between the current collector and electrode material. We confirmed that the bonding force with the current collector when a binder is used is much lower than the binding energy within the rGO electrode. The high adhesion energy of spray-rGO makes it is more stable, and hence, a more promising electrode material for flexible LIBs than slurry-rGO prepared by the conventional method.

Before applying this novel electrode to flexible LIBs, we carried out essential electrochemical measurements of the electrode in coin cells. Fig. 3 shows the charge/discharge profiles of spray-rGO at low constant current (0.1 C-rate); we conducted these experiments to understand the typical characteristics of the graphitic material [42]. In the first discharge cycle, a voltage plateau was observed at ~0.8 V because of the formation of a solid–electrolyte interface (SEI), which is a well-known phenomenon in carbon-based anode materials; it results from the reduction and decomposition of the electrolyte at the electrode surface [43]. After few charge/discharge cycles, a flat and long discharge plateau was observed at ~0.2 V, which corresponds to the intercalation of Li ions between the graphite layers [42]. Similarly, less polarization was observed in the charge profiles after the first cycle. The specific capacities of the discharge and charge steps in the 1st cycle were 466 and 334 $mAh \cdot g^{-1}$, respectively, and the irreversible capacity was approximately 132 $mAh \cdot g^{-1}$, which means the value of coulombic efficiency was 72%. The discharge/charge phases

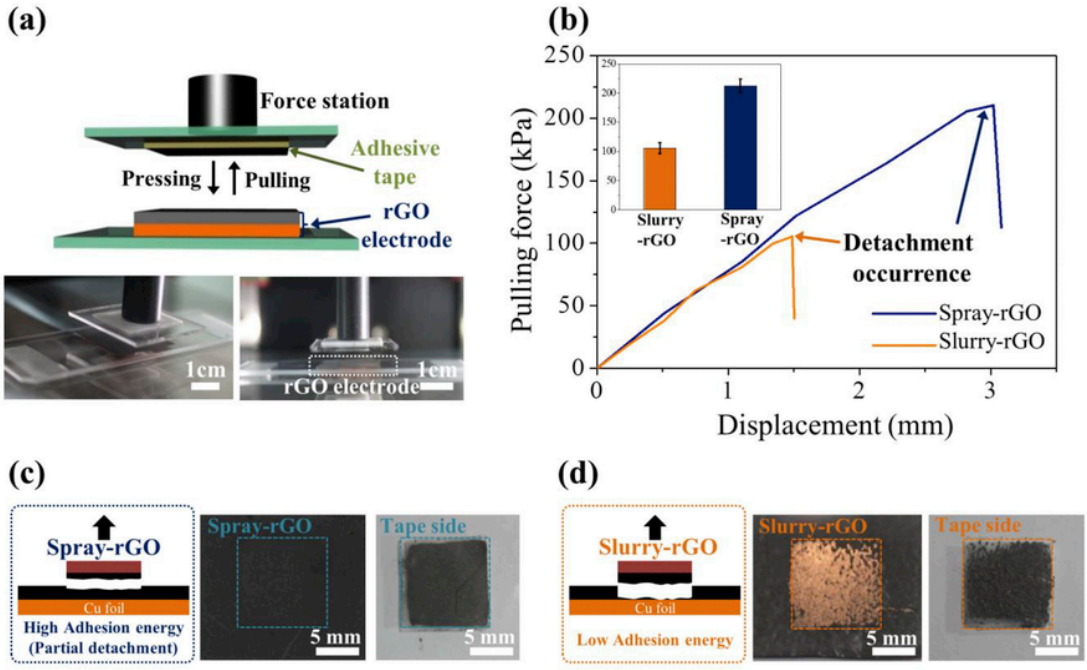

Fig. 2. (a) Schematic configuration and photographs of the system used for adhesion energy measurements of spray-rGO and slurry-rGO. (b) Adhesion measurement results for spray-rGO and slurry-rGO; arrows indicate the points where delamination occurred. The inset shows the statistics of the results with error ranges. (c–d) Schematics showing different explanations of spray-rGO and slurry-rGO and optical images of the samples after the adhesion measurements. (A colour version of this figure can be viewed online.)

of the subsequent 2nd and 3rd cycles were subsequently carried out, resulting in very flat plateaus. The coulombic efficiency in the 2nd and 3rd cycles was approximately 99%.

The charge/discharge profile of slurry-rGO is also shown in Fig. 3b for comparison with that of spray-rGO. The discharge curve in the 1st cycle of slurry-rGO also showed SEI formation at approximately 0.8 V, similar to the discharge curve of spray-rGO; its plateau was well-formed at approximately 0.2 V. In the subsequent cycles, slurry-rGO also exhibited a flat plateau and good coulombic efficiency. The irreversible capacities of the 1st cycle in both cases are compared in the inset of Fig. 3b. Spray-rGO exhibited an irreversible capacity of approximately 28%, which is 5% lower than that of slurry-rGO. This result can be explained by the following two possibilities. The first possibility is different coating densities and surface area. The SEM images shown in Fig. 1c–h confirmed that spray-rGO was denser than slurry-rGO; this difference in density can cause difference in surface area. The area of the SEI formed was proportional to the surface area; hence, greater irreversible capacity was observed in the case of slurry rGO. In this point, the lower surface area of spray-rGO can imply poorer electrochemical performance; however, the advantages of large contact area, vivid electron pathway and no-inclusion of binders can achieve higher electrochemical properties to be introduced later. The second possibility is the effect of the additives. The area of SEI formed has already been reported to depend on the binder content in carbon-based anode materials cycled at ~0.8 V vs. Li/Li^+ [13]. Therefore, the irreversible capacity of spray-rGO would be lower than that of slurry-rGO because it was fabricated without additives. Furthermore, because the additive content of slurry-rGO was 8 wt% of the total weight, except for the current collector, the gravimetric capacity of slurry-rGO was 92% of the specific capacity (Fig. 3b). This difference in gravimetric capacity is favorable for the fabrication of thin and light batteries with spray-rGO electrodes.

CV was performed to obtain detailed information about the surface kinetics and redox reactions of spray-rGO (Fig. 3c). It was performed in the voltage range of 0–2.5 V vs. Li/Li^+ at a scan rate of 0.1 mV s^{-1}. The anodic peak at ~0.5 V in the 1st cycle, which is related to SEI formation, was broad. The peak near 0 V vs. Li/Li^+ was related to intercalation, whereas the potential for deintercalation in the subsequent cathodic current was located at ~0.34 V. The peaks observed in this range indicated that Li-ion intercalation into the graphite lattice in spray-rGO clearly occurred [44]. Notably, however, the polarization decreased and the peak current increased to remarkable extents after the 2nd cycle. The cathodic peak current was 0.19 mA·cm^{-2} in the 1st cycle and increased from 0.39 to 0.53–0.75 mA·cm^{-2} in the 2nd, 3rd, and 4th cycles, respectively. This increase in the peak currents was also observed in the anodic peaks. However, the peak intensities of the anodic and cathodic currents were saturated after the 4th cycle and no further increases in cathodic and anodic peak currents were observed. In this regard, the kinetics at the interface between the rGO and the electrolyte also increased [13].

This phenomenon can be explained by the following sequential mechanism. Initially, the highly packed spray-rGO lacked sufficient access for the electrolyte–lithium intercalation; however, as charge/discharge progressed, the volume expansion of the electrode materials created a porous structure that enabled the permeation of the electrolyte into the inner space, and hence, Li^+-ion can access to the internal intercalation sites [42]. At this point, most of the plane contact area, which was strongly bonded, could maintain the overall structure; the gap created improved the accessibility of the electrolyte without structural deterioration or collapse. The SEM images of spray-rGO after the 2nd cycle are demonstrated in Fig. S3 as direct evidence. Considering SEM images, the generated gaps were formed and helped in increasing accessibility of electrolyte in the inner parts of the electrode.

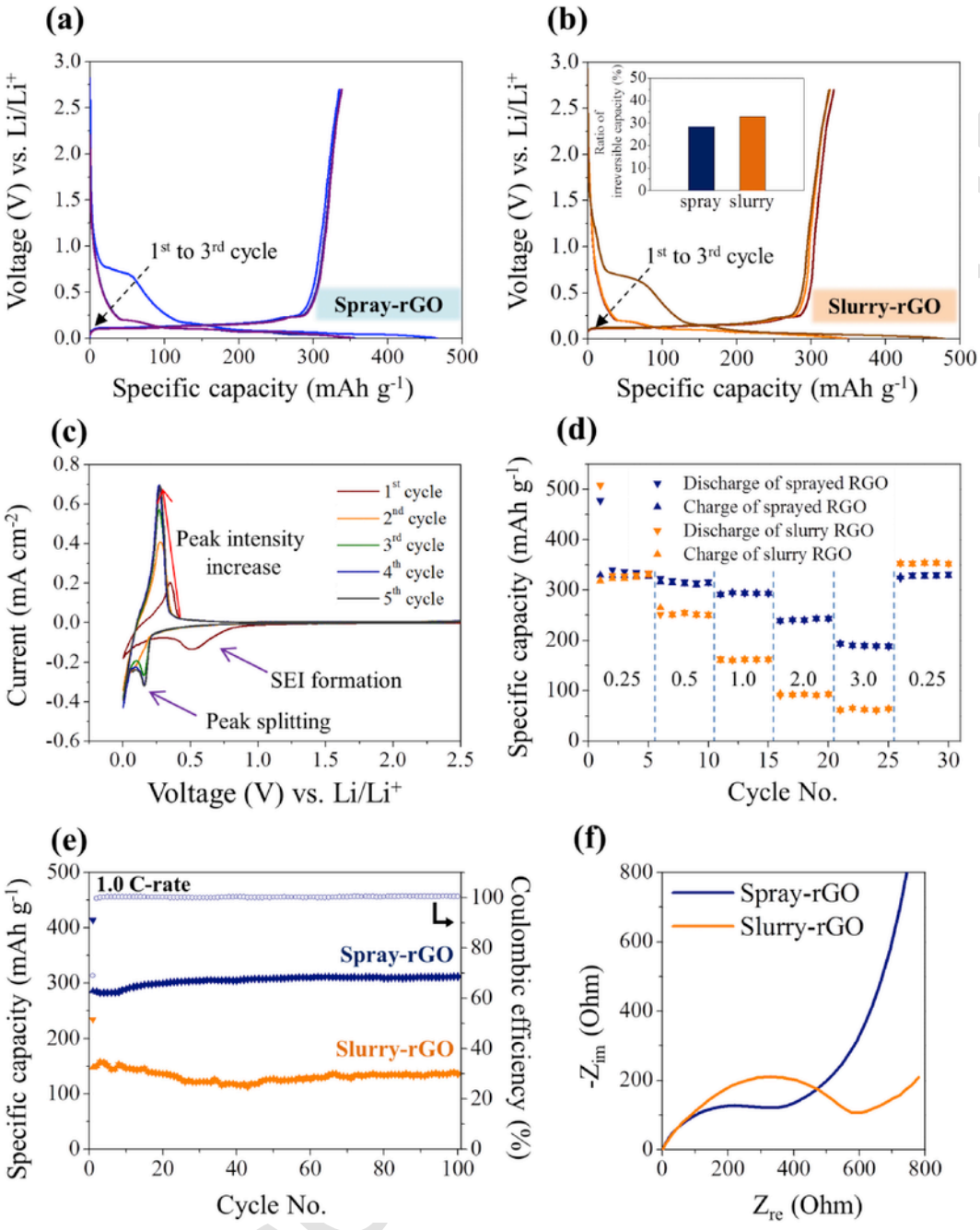

Fig. 3. (a–b) Discharge–charge profiles of (a) spray-rGO and (b) slurry-rGO within the voltage range corresponding to graphitic materials (0–2.7 V vs. Li/Li^+). The inset of (b) shows irreversible capacity of spray-rGO and slurry-rGO. (c) Cyclic voltammogram of spray-rGO at a scan rate of 0.1 mV s^{-1} between 0 and 2.5 V vs. Li/Li^+. (d) Rate capability of spray-rGO and slurry-rGO with several C-rates (0.25C, 0.5C, 1.0C, 2.0C, 3.0C, and 0.25C again). (e) Cycle performance of spray-rGO and slurry-rGO at a high C-rate (1.0C). (f) Electrochemical impedance spectroscopy results from spray-rGO and slurry-rGO. (A colour version of this figure can be viewed online.)

Therefore, the cathodic/anodic current in CV curve of spray-rGO increased during the initial cycles and reached its maximum value after complete access of the electrolyte, demonstrating that the electrode fabricated using this novel method worked perfectly in a coin cell without any collapse due to the high adhesion energy. In case of slurry-rGO, the increase and saturation in current was similarly observed in CV curve (Fig. S4) because its structure can be maintained by binders.

To compare rate-capability, the charge/discharge behaviors of both spray-rGO and slurry-rGO at different C-rates (0.25C–3C) for five cycles at each C-rate were investigated in the voltage range of 0.5–3.0 V; a lower C-rate of 0.25C was repeated after the cell was tested at 3C to confirm the structural deterioration and capacity loss due to the volumetric change and chipping-off of particles at higher C-rates (Fig. 3d). The discharge capacities of spray-rGO and slurry-rGO at 0.25C were similar: 335 and 330 mAh·g^{-1}, respectively. However, at higher C-rates (i.e., 1C, 2C, and 3C), the specific capacities of spray-rGO were 294, 248, and 190 mAh·g^{-1} and those of slurry-rGO were 162, 91, and 63 mAh·g^{-1}, respectively. Thus, at a high C-rate of 3C, the capacities of spray-rGO and slurry-rGO were 56% and

19% of their respective initial values at 0.25C, indicating that spray-rGO exhibited excellent rate capability and low capacity fading at high C-rates.

After the cells were charged/discharged at higher C-rates, they were again tested at the lower 0.25C rate to determine if the electrode structures deteriorated. Both spray-rGO and slurry-rGO recovered their initial values after cycling at high C-rates, which are severe condition for graphitic materials. Slurry-rGO, which was prepared with additives, maintained its initial capacity and structure because of the binders. By contrast, the structure and capacity of spray-rGO produced without the binder were also maintained without any collapse or detachment even after harsh high-rate charging/discharging because of the strong bonding force at the interface and within the rGO electrode. Considering the surface area that can be deduced from the irreversible capacity (inset of Fig. 3b) and SEM images (Fig. 1c–h), slurry-rGO should have better electrochemical performance, but in fact, spray-rGO has much better performances due to no-inclusion of binders, the large contact area between electrode and current collector, and smooth electron pathway inside the electrode as rGO layers are connected uniformly. Among the rate-capability results, we observed a slight increase in capacity during the 8th to 12th cycles, consistent with the CV results shown in Fig. 3c. This phenomenon may be the cause of the increase in accessibility of the electrolyte to the electrode surface during volume expansion and reduction with increasing number of charge/discharge cycles.

An extended lifecycle study was performed for spray-rGO fabricated without additives to demonstrate the stability of the electrode with increasing number of charge/discharge cycles (Fig. 3e). The cycle performance measurement in Fig. 3e was carried out at 1.0C for 100 charge/discharge cycles. The initial capacity of spray-rGO was approximately 295 $mAh \cdot g^{-1}$ and the coulombic efficiency during the 1st cycle was approximately 73%. With increasing number of cycles, a slight increase in the specific capacity was observed until the 20th cycle. This capacity increase is also consistent with the CV results in Fig. 3c and with the rate-capability results in Fig. 3d. The phenomenon equally occurred in all experiments shown in Fig. 3c–e, presumably because of the high density of spray-rGO. However, even portions of the spray-rGO electrode provided electrolyte accessibility because of volume expansion/contraction; the bottom part remained in contact with the Cu surface with very high adhesion energy. Therefore, after the capacity increased during the initial 20 cycles, the specific capacities of spray-rGO from the 20th cycle to the 100^{th} cycle were sustained, with no capacity loss or degradation even at a relatively high C-rate (1.0C). Fan et al. observed this phenomenon in a previous study related to carbon nanotube sheets with SnO_2 nanoparticles [45]. By contrast, the cycle performance results for the slurry-rGO fabricated with additives showed an initial capacity of 150 $mAh \cdot g^{-1}$, which is approximately 40% of the capacity at 0.25C, and its long-term cycling efficiency became very unstable under the high-rate condition. The slurry-rGO electrode structure provided an electron pathway via conductor particles between the rGO particles; however, this pathway could not serve a smooth electron pathway at high C-rates because of the narrow contact area at the interface between the active material and current collector, which may be the reason for the instability of slurry-rGO. The rate capability and cycle performance of spray-rGO were determined to be suitable for real LIB applications.

The EIS results in Fig. 3f were obtained for both spray-rGO and slurry-rGO to confirm a direct basis for the improved electrochemical characteristics of spray-rGO. From the EIS results, the charge transfer resistance, R_{ct}, of spray-rGO and slurry-rGO was 382 and 601 Ω, respectively. The lower R_{ct} of spray-rGO, which exhibits better electronic conductivity than that of slurry-rGO, promotes fast charge and discharge processes. The lower value of R_{ct} in the case of spray-rGO is due to the absence of binder which can induce lower conductivity [46]. Hence, spray-rGO exhibits better rate capability, as previously discussed.

To compare the performance of spray-rGO, we compared the results with those for rGO, as reported by other authors; the relevant information is given in Fig. S5 [47–51]. In the case of rGO, the defect and impurity levels were high because of chemical exfoliation near the graphene layers; the irreversible capacities at the 1st cycle were approximately 40%–80% (Fig. S5a) [40,47–51]. By contrast, the irreversible capacities of spray-rGO were minimal compared to those reported in the literature. To compare the rate capability with those in previous reports, data corresponding to different C-rates are compared in Fig. S5b [47–51]. The best rate capability in previous studies was exhibited by pyrolysis rGO [50] as an anode for LIBs, which showed capacity retention of approximately 58% at the 3C rate relative to that at the 0.25C rate. However, our results demonstrated that spray-rGO exhibits better performance, with 62% even in the absence of dopants or additives because of its large contact area, which provides a smooth electron pathway.

The electrochemical properties of spray-rGO as an anode material for LIBs were evaluated using a half-cell. Spray-rGO demonstrated excellent rate capability and cycle life when Li metal was used as a counter/reference electrode. We further used spray-rGO as a flexible electrode for flexible LIBs. As shown in Fig. 4a, the configuration of the flexible LIB was PDMS sealant/spray-rGO on a Cu current collector as the anode/PE film as a separator/$LiCoO_2$ (LCO) electrode on an Al current collector as the cathode/PDMS sealant. After all components were stacked, the electrolyte was injected via a syringe. The flexible LIBs were fabricated in an Ar-filled glovebox. As shown in the inset of Fig. 4a, the spray-rGO electrode fabricated without binders was bent with bending radius (R_c) of ~5 mm, but no cracking or damage was observed. The SEM images in Fig. S6 provide detailed information about the bent spray-rGO and slurry-rGO electrodes bent using various R_c values. Neither spray-rGO nor slurry-rGO showed delamination when R_c was 1 mm. When R_c was decreased to ~200 μm, which is close to folding, no cracking or delamination was observed at the surface of spray-rGO, whereas the surface of slurry-rGO showed cracks along most of the bent line and delamination or loss of the rGO electrode material. The greater flexibility of spray-rGO compared with that of slurry-rGO is attributed to the strong adhesion energy, which enables mechanical flexibility in an LIB [12]. As a result, a flexible LIB with a spray-rGO anode was successfully assembled and possessed good flexibility in terms of total structure (Fig. 4b).

After the spray-rGO flexible LIB was charged, the battery could independently sustain a blue light-emitting diode (LED) without any external circuit, as shown in Fig. 4c. The video clip in the Supporting Information confirms that the flexible LIB fabricated with spray-rGO and a PDMS package can stably turn on the LED in both flexed and twisted states as well as in the maximum bending state. For a more detailed electrochemical characterization, the cycle performance of the spray-rGO flexible LIB at various bending radii—specifically, the flat (∞), 24 mm, 16 mm, 8 mm, and again flat state at 1.5 C-rate—are demonstrated in Fig. 4d. The initial capacity of the flexible LIB fabricated using additive-free spray-rGO was approximately 242 $mAh \cdot g_{rGO}^{-1}$ in the flat state, and its capacities were maintained without significant fluctuation or degradation during a ten-cycle interval. From the 11th to 40^{th} cycle, the flexible LIB was bent with R_c = 24, 16 and 8 mm, where it exhibited specific capacities of 240–241 $mAh \cdot g_{RGO}^{-1}$ in both bending states, with no capacity deterioration. The structural stability in the recovery state from the 41^{th} to 50^{th}

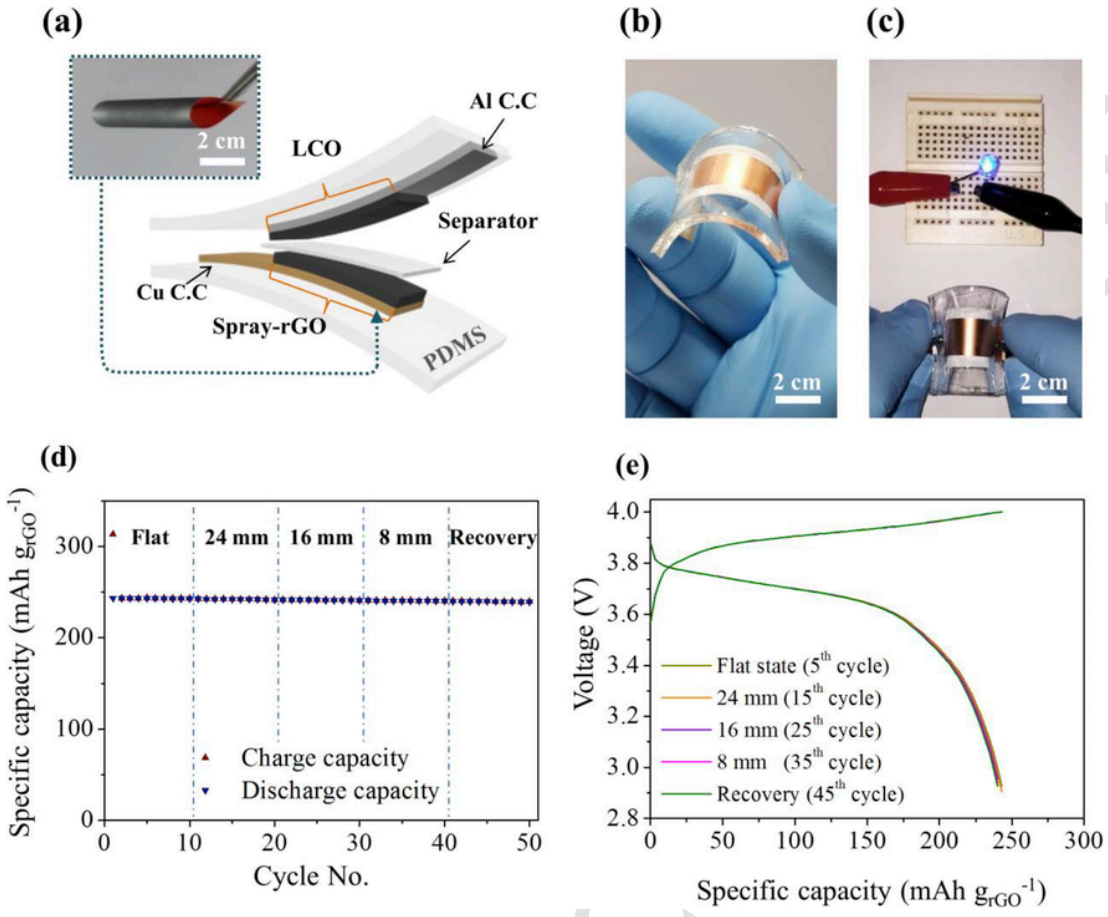

Fig. 4. (a) Schematic of a flexible LIB with spray-rGO as an anode (configuration: PDMS/spray-rGO/separator/LCO electrode/PDMS). The inset photograph shows a bent spray-rGO electrode with a bending radius of 5 mm. (b) Photograph of a spray-rGO flexible LIB in the bent state. (c) Demonstration of the spray-rGO flexible LIB turning on a blue LED while in the bent state. (d) Cycle performance of flexible LIB composed of spray-rGO as an anode at various bending states. (e) Charge–discharge profiles of representative cycles (5th, 15th, 25th, 35th, and 45th) of a flexible LIB with spray-rGO. (A colour version of this figure can be viewed online.)

cycle was also confirmed. This recovery step, where the initial capacity is restored with no change, demonstrates the excellent flexibility of the spray-rGO. The flexible LIB using slurry-rGO as an electrode showed poor flexibility in bending/flexible states as shown in Fig. S7a. Comparing the spray-rGO and slurry-rGO (Fig. S7b), spray-rGO possessed high flexibility without changing its initial capacity in bending. On the other hand, the flexible LIB with slurry-rGO showed that its capacities decrease as the bending step changed, and when it finally flattened again at the end(recovery step), its capacity did not return to the initial values.

Supplementary video related to this article can be found at https://doi.org/10.1016/j.carbon.2018.06.040.

The flexibility tests of the flexible LIB confirmed that the high adhesion energy resulted in good adhesion with no chipping-off or delamination of particles from the current collector even though the electrode was subjected to high strain. As shown in the representative discharge/charge profiles corresponding to various bending states (Fig. 4e), the tips of the discharge curves were slightly reduced. Because the capacity was gradually decreased to the recovery state independent of the bending state, this decrease might be caused by electrolyte consumption through the porous structure of PDMS. That is, chipping-off or delamination of electrode particles did not occur during the flexibility demonstration. The binder-free spray-rGO electrode, in which the active material layer was strongly adhered to the current collector, exhibited good electrochemical characteristics and high flexibility. Therefore, the novel electrode manufacturing process used to fabricate the spray-rGO electrode is a promising process for the future development of flexible LIBs for flexible electronic devices.

4. Conclusions

In summary, the additive-free spray-rGO electrode fabrication process using a supersonic kinetic spray was investigated and demonstrated for flexible, lightweight, and high-power LIBs. The results confirm not only the viability of additive-free electrode fabrication induced by the supersonic kinetic spray with high kinetic energy but also that the fabricated electrodes exhibit excellent mechanical flexibility because of its high adhesion energy. The cells fabricated using additive-free spray-rGO electrodes displayed outstanding electrochemical performance in terms of high rate-capability and long-term cycle performance due to the enlarged contact area at the interface between the current collector and the electrode and the electrochemical performance of the spray-rGO in LIBs was not affected by bending or twisting conditions. If the novel approach of supersonic kinetic spray-based electrode fabrication process is combined with other strategies such as porous, nanostructured, or carbon-based current collectors, the adhesion energy between the electrode and current collector can be maximized for achieving extremely high flexibility. Furthermore this electrode fabrication strategy has potential for the

large-scale and industrial fabrication using a continuous roll-to-roll spraying process, and its application range can be potentially extended to the additive-free fabrication of other anode and cathode materials. Therefore, this novel approach is expected to be a key technology for the fabrication of flexible electrodes and to strongly affect the field of flexible batteries for powering future electronics.

Acknowledgements

This work was supported by the National Research Foundation of Korea (NRF-2015R1A3A2066337 and CASE2014M3A6A5060933) funded by the Ministry of Science and ICT of Korea.

Appendix A. Supplementary data

Supplementary data related to this article can be found at https://doi.org/10.1016/j.carbon.2018.06.040.

Uncited reference

[38].

References

[1] L. Li, Z. Wu, S. Yuan, X.-B. Zhang, Advances and challenges for flexible energy storage and conversion devices and systems, Energy Environ. Sci. 7 (2014) 2101–2122.
[2] A.S. Aricò, P. Bruce, B. Scrosati, J.-M. Tarascon, W. van Schalkwijk, Nanostructured materials for advanced energy conversion and storage devices, Nat. Mater. 4 (2005) 366–377.
[3] M. Winter, R.J. Brodd, What are batteries, fuel cells, and supercapacitors?, Chem. Rev. 104 (2004) 4245–4270.
[4] K. Rana, J. Singh, J.-H. Ahn, A graphene-based transparent electrode for use in flexible optoelectronic devices, J. Mater. Chem. C 2 (2014) 2646–2656.
[5] Y.-H. Zhu, s Yuan, D. Bao, Y.-B. Yin, H.-X. Zhong, X.-B. Zhang, J.-M. Yang, Q. Jinag, Decorating waste cloth via industrial wastewater for tube-type flexible and wearable sodium-ion batteries, Adv. Mater. 29 (2017) 1603719.
[6] T. Liu, J.-J. Xu, Q.-C. Liu, Z.-W. Chang, Y.-B. Yin, X.-Y. Yang, X.-B. Zhang, Ultrathin, lightweight, and wearable Li-O_2 battery with high robustness and gravimetric/volumetric energy density, Small 13 (2017) 1602952.
[7] H. Gwon, H.-S. Kim, K.U. Lee, D.-H. Seo, Y.C. Park, Y.-S. Lee, et al., Flexible energy storage devices based on graphene paper, Energy Environ. Sci. 4 (2011) 1277–1283.
[8] M.-S. Balogun, W. Qui, F. Lyu, Y. Luo, H. Meng, J. Li, et al., All-flexible lithium ion battery based on thermally-etched porous carbon cloth anode and cathode, Nano Energy 26 (2016) 446–455.
[9] J.-M. Tarascon, M. Armand, Issues and challenges facing rechargeable lithium batteries, Nature 414 (2001) 359–367.
[10] C. Sun, J. Liu, Y. Gong, D.P. Wilkinson, J. Zhang, Recent advances in all-solid-state rechargeable lithium batteries, Nano Energy 33 (2017) 363–386.
[11] M.-H. Ryou, J. Kim, I. Lee, S. Kim, Y.K. Jeong, S. Hong, et al., Mussel-inspired adhesive binders for high-performance silicon nanoparticle anodes in lithium-ion batteries, Adv. Mater. 25 (2013) 1571–1576.
[12] K. Wang, S. Luo, Y. Wu, X. He, F. Zhao, J. Wang, et al., Super-aligned Carbon nanotube films as current collectors for lightweight and flexible lithium ion batteries, Adv. Funct. Mater. 23 (2013) 846–853.
[13] S. Flandrois, B. Simon, Carbon materials for lithium-ion rechargeable batteries, Carbon 37 (1999) 165–180.
[14] L. Fransson, T. Eriksson, K. Edström, T. Gustafsson, J.O. Thomas, Influence of carbon black and binder on Li-ion batteries, J. Power Sources 101 (2001) 1–9.
[15] P.L. Taberna, S. Mitra, P. Poizot, P. Simon, J.-M. Tarascon, High rate capabilities Fe_3O_4-based Cu nano-architectured electrodes for lithium-ion battery applications, Nat. Mater. 5 (2006) 567–573.
[16] M. Yao, K. Okuno, T. Iwaki, M. Kato, S. Tanase, K. Emura, et al., $LiFePO_4$-based electrode using micro-porous current collector for high power lithium ion battery, J. Power Sources 173 (2007) 545–549.
[17] S.R. Gowda, A.L.M. Reddy, X. Zhan, H.R. Jafry, P.M. Ajayan, 3D nanoporous nanowire current collectors for thin film microbatteries, Nano Lett. 12 (2012) 1198–1202.
[18] S. Zhang, Z. Du, R. Lin, T. Jiang, G. Liu, X. Wu, et al., Nickel nanocone-array supported silicon anode for high-performance lithium ion batteries, Adv. Mater. 22 (2010) 5378–5382.
[19] C. Arbizzani, M. Lazzari, M. Mastragostino, Lithiation/delithiation performance of Cu_6Sn_5 with carbon paper as current collector, J. Electrochem. Soc. 152 (2005) A289–A294.
[20] J. Guo, A. Sun, C. Wang, A porous silicon–carbon anode with high overall capacity on carbon fiber current collector, Electrochem. Commun. 12 (2010) 981–984.
[21] J.W. Choi, L. Hu, L. Cui, J.R. McDonough, Y. Cui, Metal current collector-free freestanding silicon–carbon 1D nanocomposites for ultralight anodes in lithium ion batteries, J. Power Sources 195 (2010) 8311–8316.
[22] S.K. Marth, J.O. Kiggans, J. Nanda, N.J. Dudney, Advanced lithium battery cathodes using dispersed carbon fibers as the current collector, J. Electrochem. Soc. 158 (2011) A1060–A1066.
[23] L. Hu, H. Wu, F. La Mantia, Y. Yang, Y. Cui, Thin, flexible secondary Li-ion paper batteries, ACS Nano 4 (2010) 5843–5848.
[24] J.C. Lytle, J.M. Wallace, M.B. Sassin, A.J. Barrow, J.W. Long, J.L. Dysart, et al., The right kind of interior for multifunctional electrode architectures: carbon nanofoam papers with aperiodic submicrometre pore networks interconnected in 3D, Energy Environ. Sci. 4 (2011) 1913–1925.
[25] S.H. Ng, J. Wang, Z.P. Guo, J. Chen, G.X. Wang, H.K. Liu, Single wall carbon nanotube paper as anode for lithium-ion battery, Electrochim. Acta 51 (2005) 23–28.
[26] X.-Y. Yang, J.-J. Xu, D. Bao, Z.-W. Chang, D.-P. Liu, Y. Zhang, X.-B. Zhang, High-performance integrated self-package flexible Li–O_2 battery based on stable composite anode and flexible gas diffusion layer, Adv. Mater. 29 (2017) 1700378.
[27] X.-Y. Yang, J.-J. Xu, Z.-W. Chang, D. Bao, Y.-B. Yin, T. Liu, J.-M. Yan, D.-P. Liu, Y. Zhang, X.-B. Zhang, Blood-capillary-inspired, free-standing, flexible, and low-cost super-hydrophobic N-CNTs@SS cathodes for high-capacity, high-rate, and stable Li-air batteries, Adv. Energy Mater 8 (2018) 1702242.
[28] L. Shen, E. Uchaker, X. Zhang, G. Cao, Hydrogenated $Li_4Ti_5O_{12}$ nanowire arrays for high rate lithium ion batteries, Adv. Mater. 24 (2012) 6502–6506.
[29] Y.-H. Zhu, Y.-B. Yin, X. Yang, T. Sun, S. Wang, Y.-S. Jiang, J.-M. Yan, X.-B. Zhang, Transformation of rusty stainless-steel meshes into stable, low-cost, and binder-free cathodes for high-performance potassium-ion batteries, Angew. Chem. Int. Ed. 56 (2017) 7881–7885.
[30] S.D. Kim, K. Rana, J.-H. Ahn, Additive-free synthesis of $Li_4Ti_5O_{12}$ nanowire arrays on freestanding ultrathin graphite as a hybrid anode for flexible lithium ion batteries, J. Mater. Chem. A 4 (2016) 19197–19206.
[31] Y. Bao, X. Zhang, X. Zhang, L. Yang, X. Zhang, H. Chen, et al., Free-standing and flexible $LiMnTiO_4$/carbon nanotube cathodes for high performance lithium ion batteries, J. Power Sources 321 (2016) 120–125.
[32] K. Rana, J. Singh, J.T. Lee, J.H. Park, J.-H. Ahn, Highly conductive freestanding graphene films as anode current collectors for flexible lithium-ion batteries, ACS Appl. Mater. Interfaces 6 (2014) 11158.
[33] K. Rana, S.D. Kim, J.-H. Ahn, Additive-free thick graphene film as an anode material for flexible lithium-ion batteries, Nanoscale 7 (2015) 7065–7071.
[34] D.-Y. Kim, S. Sinha-Ray, J.J. Park, J.-G. Lee, Y.-H. Cha, S.-H. Bae, et al., Self-healing reduced graphene oxide films by supersonic kinetic spraying, Adv. Funct. Mater. 24 (2014) 4986–4995.
[35] C.N.R. Rao, A.K. Sood, K.S. Subrahmanyam, A. Govindaraj, Graphene: the new two-dimensional nanomaterial, Angew. Chem. Int. Ed. 48 (2009) 7752–7777.
[36] M. Winter, J.O. Besenhard, M.E. Spahr, P. Novák, Insertion electrode materials for rechargeable lithium batteries, Adv. Mater. 10 (1998) 725–763.
[37] A.C. Ferrari, J.C. Meyer, V. Scardaci, C. Casiraghi, M. Lazzeri, F. Mauri, et al., Raman spectrum of graphene and graphene layers, Phys. Rev. Lett. 97 (2006) 187401.
[38] Z.H. Ni, T. Yu, Y.H. Lu, Y.Y. Wang, Y.P. Feng, Z.X. Shen, Uniaxial strain on graphene: Raman spectroscopy study and band-gap opening, ACS Nano 2 (2008) 2301–2305.
[39] K.N. Kudin, B. Ozbas, H.C. Schniepp, R.K. Prud'homme, I.A. Aksay, R. Car, Raman spectra of graphite oxide and functionalized graphene sheets, Nano Lett. 8 (2008) 36–41.
[40] C.B. Robledo, M. Otero, G. Luque, O. Cámara, D. Barraco, M.I. Rojas, et al., First-principles studies of lithium storage in reduced graphite oxide, Electrochim. Acta 140 (2014) 232–237.
[41] G. Wang, X. Shen, J. Yao, J. Park, Graphene nanosheets for enhanced lithium storage in lithium ion batteries, Carbon 47 (2009) 2049–2053.
[42] N.A. Kaskhedikar, J. Maier, Lithium storage in carbon nanostructures, Adv. Mater. 21 (2009) 2664–2680.
[43] V. Eshkenazi, E. Peled, L. Burstein, D. Golodnitsky, XPS analysis of the SEI formed on carbonaceous materials, Solid State Ionics 170 (2004) 83–91.
[44] V. Etacheri, R. Marom, R. Elazari, G. Salitra, D. Aurbach, Challenges in the development of advanced Li-ion batteries: a review, Energy Environ. Sci. 4 (2011) 3243–3262.

[45] H.-X. Zhang, C. Feng, Y.-C. Zhai, K.-L. Jiang, Q.-Q. Li, S.-S. Fan, Cross-stacked carbon nanotube sheets uniformly loaded with SnO_2 nanoparticles: a novel binder-free and high-capacity anode material for lithium-ion batteries, Adv. Mater. 21 (2009) 2299–2304.
[46] M. Yoo, C.W. Frank, S. Mori, S. Yamaguchi, Effect of poly(vinylidene fluoride) binder crystallinity and graphite structure on the mechanical strength of the composite anode in a lithium ion battery, Polymer 44 (2003) 4197–4204.
[47] Z.-S. Wu, W. Ren, L. Xu, F. Li, H.-M. Cheng, Doped graphene sheets as anode materials with superhigh rate and large capacity for lithium ion batteries, ACS Nano 5 (2011) 5463–5471.
[48] H. Cao, X. Zhou, C. Zheng, Z. Liu, Metal etching method for preparing porous graphene as high performance anode material for lithium-ion batteries, Carbon 89 (2015) 41–46.
[49] C. Hu, X. Zhai, L. Liu, Y. Zhao, L. Jiang, L. Qu, Spontaneous reduction and assembly of graphene oxide into three-dimensional graphene network on arbitrary conductive substrates, Sci. Rep. 3 (2013) 2065.
[50] J. Yang, Q. Liao, X. Zhou, X. Liu, J. Tang, Efficient synthesis of graphene-based powder via in-situ spray pyrolysis and its application in lithium ion batteries, RSC Adv. 3 (2013) 16449–16455.
[51] M. Kim, D.Y. Kim, Y. Kang, O.O. Park, Facile fabrication of highly flexible graphene paper for high-performance flexible lithium ion battery anode, RSC Adv. 5 (2015) 3299–3305.